ACS Macro Letters

Letter

pubs.acs.org/macroletters

Three-Dimensional Writing of Highly Stretchable Organic Nanowires

Ji Tae Kim,[†] Jaeyeon Pyo,[†] Jonghyun Rho,[‡] Jong-Hyun Ahn,[‡] Jung Ho Je,*[,†] and G. Margaritondo*[,§]

[†]X-ray Imaging Center, Department of Materials Science and Engineering, Pohang University of Science and Technology, Pohang 790-784, Korea

[‡]School of Advanced Materials Science and Engineering, SKKU Advanced Institute of Nanotechnology, Sungkyunkwan University, Suwon 440-746, Korea

[§]Faculté des Sciences de Base, Ecole Polytechnique Fédérale de Lausanne (EPFL), CH-1015 Lausanne, Switzerland

Supporting Information

ABSTRACT: Three-dimensional (3D) writing is a promising approach to realize stretchable electronics, but is so far limited to microscale features. We developed accurate 3D writing for highly stretchable organic nanowire arrays using a nanoscale polymer meniscus. Specifically, 3D nanoarches of poly(3,4-ethylenedioxythiophene)/poly(styrenesulfonate) with unprecedented stretchability, over 270%, and no compromise on the electrical characteristics were fabricated. Then, we integrated nanoarches into photoswitches, electrochemical transistors, and electrical interconnects. The impact of these successful tests goes well beyond these specific devices and opens the way to new classes of stretchable nanodevices based on organic materials.

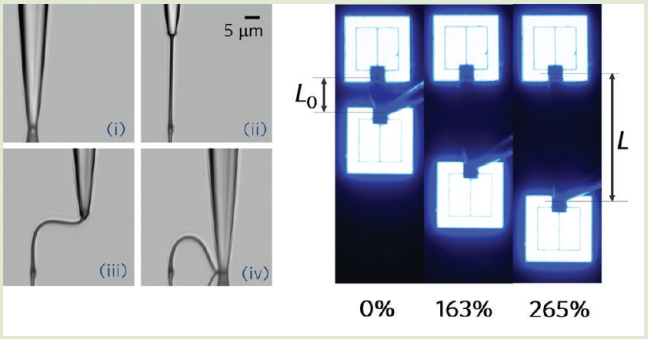

Stretchable electronics attracts a great deal of attention because of the potential applications in a variety of areas ranging from robotic sensory skins and wearable communication systems to bioelectronic devices.[1−7] One of the most important challenges is the realization of high stretchability in different classes of nanomaterials.[8−12]

Recently, two innovative strategies have been employed to obtain high stretchability in nanomaterials: one is to increase intrinsic stretchabilities of materials and the other is to design stretchable architectures.[1,13] The latter strategy attracts huge attention because stretchable architectures, for instance, wavy shapes in nanomaterials can accommodate, similar to an accordion bellows, large applied strains without significant degradation in electrical properties.[11]

Mechanical buckling is a typical method to realize stretchable wavy or coil shapes in nanosystems such as silicon nanowires,[8,9] nanoribbons,[10,11] and carbon nanotubes.[12] This led, for example, to an impressive 100% stretchability for Si nanowire coils. However, omnidirectional and individual integration of such nanosystems that is indispensable for the fabrication of real stretchable nanodevices still remains a formidable challenge.

One impressive approach was suggested to overcome the above challenge: direct ink three-dimensional (3D) writing based on the extrusion of concentrated colloidal ink through a nozzle.[14−16] This method enables one to realize omnidirectional and individual integration of 3D stretchable architectures with wavy or arch shapes. However, bringing the integration below micrometer-level still remains a challenge because of the limitations in controlling the size and the concentration of the ink particles.[14]

Conjugated polymers are promising materials in electronics,[17] photonics,[18] and bioelectronics[19−22] because of their excellent electrical and optical properties and biocompatibility. In particular, conjugated polymer nanowires are quite important building blocks for a broad range of nanodevices. To make such nanodevices flexible and stretchable, high stretchability is required for each nanowire. Existing patterning methods such as soft lithography,[23,24] dip-pen lithography,[25] and electrospinning[26] are generally limited to in-plane nanostructures with tensile fracture strain <5%, insufficient for stretchable electronics.[27]

We present here an alternate approach: the use of three-dimensional (3D) writing based on guiding a nanoscale polymer meniscus to produce highly stretchable conjugated polymer nanowire arrays. This method is particularly effective for nanoscale 3D integration[28] which is quite difficult with previous 3D micropatterning methods such as direct ink writing[14] and probe-based drawing.[29] Here we successfully fabricated 3D nanostructures of poly(3,4-ethylenedioxythiophene)/poly(styrenesulfonate) (PEDOT/PSS) not only with omnidirectional integration and site-specific positioning, but also with controlled dimensions and individually tunable electrical transport properties. These structures included 3D

Received: December 28, 2011
Accepted: February 7, 2012
Published: February 21, 2012

   dx.doi.org/10.1021/mz200249c | *ACS Macro Lett.* 2012, 1, 375−379

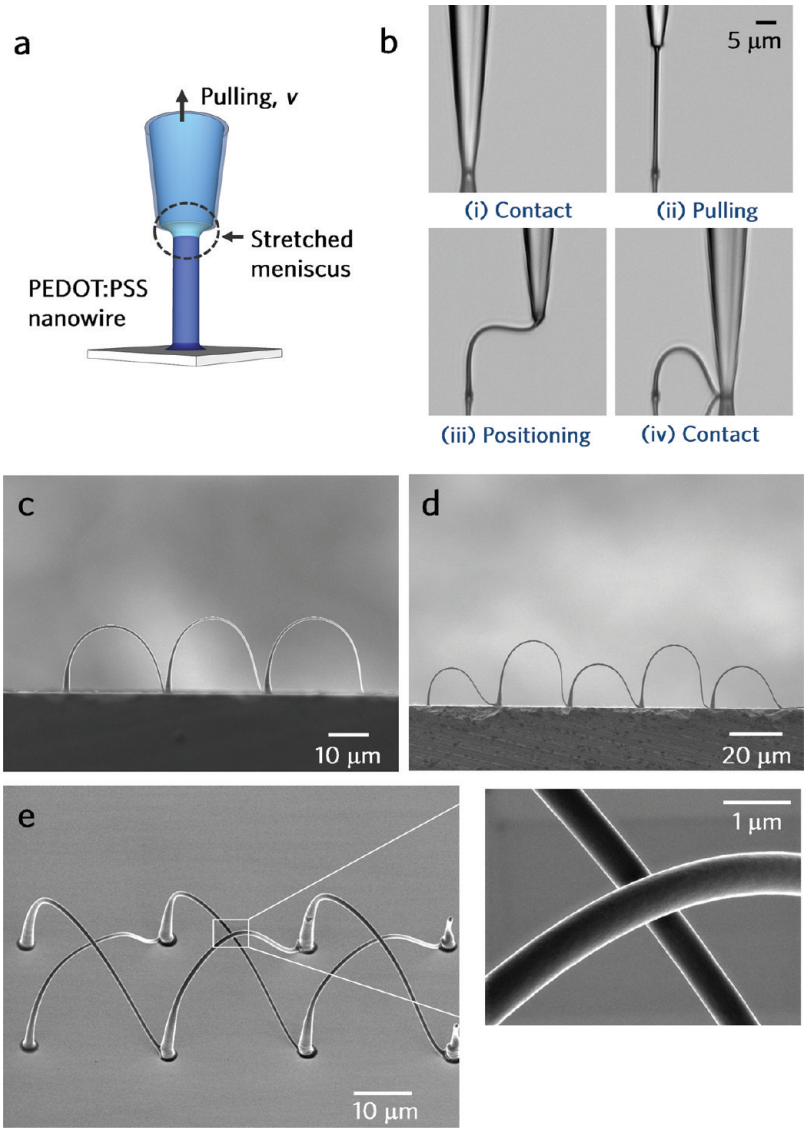

Figure 1. Formation of 3D PEDOT/PSS nanoarches. (a) Scheme of the fabrication method. (b) Optical micrographs of the fabrication steps. (c–e) 3D writing of PEDOT/PSS nanoarch arrays with controlled dimensions and accurate individual positioning. FE-SEM images of (c) a series of uniform nanoarches with 200 nm radius on a Pt substrate; (d) a nanoarch array with accurately controlled alternating arc lengths of 50 and 62.5 μm; and (e) an array of 3D nanojunctions. (Inset) A magnified FE-SEM image of the nanojunction.

nanoarches that combined unprecedented stretchability above 270% and excellent transport and photoconductivity characteristics. Such nanoarches were then successfully tested as components of different nanodevices operating under extreme stretching conditions.

Figure 1a schematically illustrates the fabrication method (for the details, see the Experimental Methods). In short, when the micropipet touches the substrate, a PEDOT/PSS liquid meniscus is created at its opening. As the micropipet is pulled away, the meniscus is stretched, its cross section decreases down to nanoscale, and the solvent (water) evaporates, yielding a PEDOT/PSS nanowire (Figure 1a). By continuing to pull, a freestanding, high-aspect-ratio PEDOT/PSS nanostructure is fabricated.

Variations of this method yield different nanowire-based structures. The optical micrograph sequence of Figure1b shows the four-step creation of a nanoarch: (i) initial contact to form the first foot; (ii) pulling; (iii) and (iv) positioning and contact for the second foot. The FE-SEM image in Figure 1c shows simple and uniform nanoarches with a radius of 200 nm and a constant arc length of 46 μm on a Pt substrate. The arc length can be individually and accurately controlled: Figure 1d shows, for example, a series of nanoarches with alternating lengths of 50 and 62.5 μm. Another interesting example is the 3D nanojunction array of Figure 1e, demonstrating omnidirectional integration and site-specific positioning.

By tuning the pulling speed, v, we were also able to accurately control the nanoarch radius, r. The radius r is related to the pulling speed v and to W, the flow rate of the polymer solution through the pipet opening, also a function of v, by the material balance law[28]

$$r = \left(\frac{W(v)}{\pi v}\right)^{1/2} \quad (1)$$

Figure 2a shows the $r-v$ dependence for a micropipet radius r_0 = 750 nm: r decreases from 675 to 135 nm as v increased from 12.5 to 750 μm/s. The solid line corresponds to a functional

dx.doi.org/10.1021/mz200249c | ACS Macro Lett. 2012, 1, 375–379

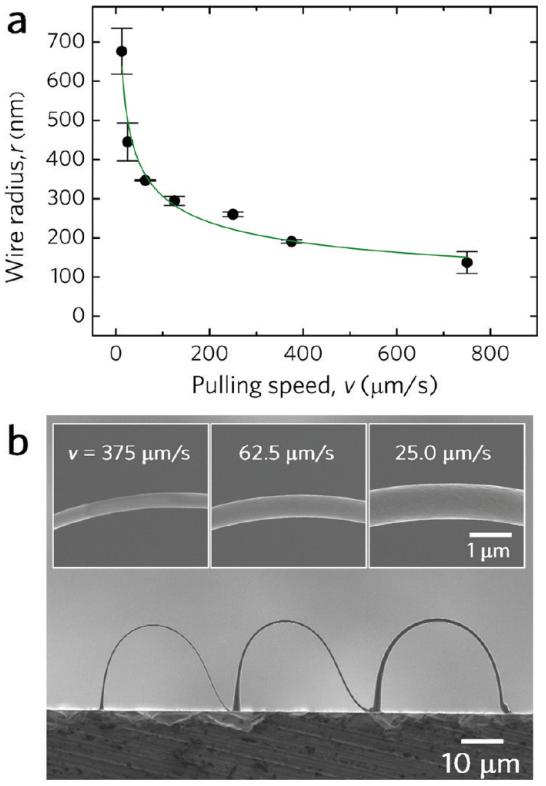

Figure 2. Controlled wire radius with pulling speed. (a) Plot of the wire radius, r, vs the pulling speed, v, for a pipet radius r_0 = 750 nm. The solid line is the best fit with $r \sim v^{-0.35}$. (b) FE-SEM images of a PEDOT/PSS nanoarch array with individually controlled radii of 195, 335, and 495 nm by tuning the pulling speed during the growth.

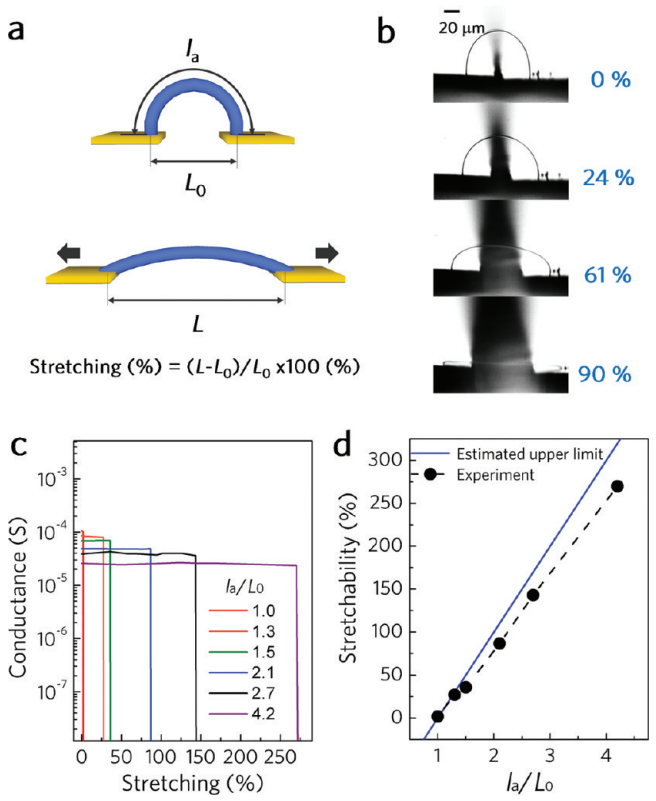

Figure 3. Stretchable nanoarches. (a) Scheme of stretching tests using two electrodes embedded in PDMS. Larger l_a/L_0 ratios correspond to higher stretchability. (b) A series of optical micrographs showing the stretching up to ~90% of a l_a/L_0 = 1.92 nanoarch. (c) Conductance vs stretching level (defined as $(L - L_0)/L_0 \times 100\%$) for different l_a/L_0 ratios. (d) Stretchability (defined as the stretching $(L - L_0)/L_0 \times 100\%$ at breakage) vs l_a/L_0. We obtained stretchability levels over 270%.

dependence $r \sim v^{-0.35}$. The flow rate W, estimated using eq 1, increases with v as $W(v) \sim v^{0.3}$ (Supporting Information, Figure S1) due to the enhancement of the pressure on the polymer solution.[28] The FE-SEM image of Figure 2b illustrates a successful test of individual control of the nanoarch radius during a serial growth. The radius was 495, 335, and 195 nm, as v varied from 25.0 to 62.5 and to 375 μm/s (see the insets of Figure 2b).

The key result of our study was, of course, the high stretchability level, defined as the stretching $(L - L_0)/L_0 \times 100\%$ at breakage (where L and L_0 = stretched and unstretched distances between the two feet (see Figure 3a)). The stretchability is expected to increase with the l_a/L_0 ratio, where l_a is the arc length; this was confirmed by measurements on ~400 nm radius nanoarches grown between two Pt-coated Si wafers embedded in PDMS (polydimethylsiloxane). A series of optical micrographs in Figure 3b show the stretching of a nanoarch with l_a/L_0 = 1.92; this specific nanoarch had a stretchability ~90%.

How much can the nanoarches be stretched with no deterioration of the electrical properties? To answer this key question, we measured the conductance during stretching. The conductivity was controlled from 10^{-2} to 200 S/cm using two types of PEDOT/PSS plus dimethyl sulfoxide (DMSO) as a secondary dopant (Supporting Information, Figure S2). The plots in Figure 3c show the results for nanoarches (made of high conductivity grade PEDOT/PSS with 2.0 wt % DMSO) with 400 nm radius and different l_a/L_0 ratios in the 1.0 - 4.2 range.

The conductivity, 200 S/cm, is independent of l_a/L_0 (see Supporting Information, Figure S3). One important result is that the nanoarch conductance stays constant during stretching (Figure 3c) until foot breakage. This proves our 3D nanoarches combine high stretchability with good electronic performances. This is of course a very interesting feature for stretchable electronics applications.

Figure 3d confirms the correlation between stretchability and the l_a/L_0 ratio, suggesting a proportionality law. The maximum stretchability from our measurements was 270% for l_a/L_0 = 4.2, a level ~50 times larger than for the intrinsic stretchability of PEDOT/PSS.[27] The experimental data of Figure 3d are close to the estimated upper limit, $(l_a - L_0)/L_0 \times 100\%$.

The integration of our stretchable nanoarches in real active devices was successfully demonstrated for photoswitches and electrochemical transistors (ECTs). Figure 4a schematically shows stretchable photoswitches using normal conductivity PEDOT/PSS, 1.3 wt %: a nanoarch bridged two Au electrodes embedded in PDMS. Figure 4b shows the photocurrent during a series of light pulses with 30 min^{-1} frequency by a 633 nm wavelength laser (a 20 V voltage was applied across Au–Au electrodes). The rapid switching was not significantly affected by 78 and 105% stretching. The on/off ratios changed slightly probably due to changes in the laser illumination. Stretchable photoswitches of this kind could be used, for example, for retinal prosthetic devices.[30]

dx.doi.org/10.1021/mz200249c | ACS Macro Lett. 2012, 1, 375–379

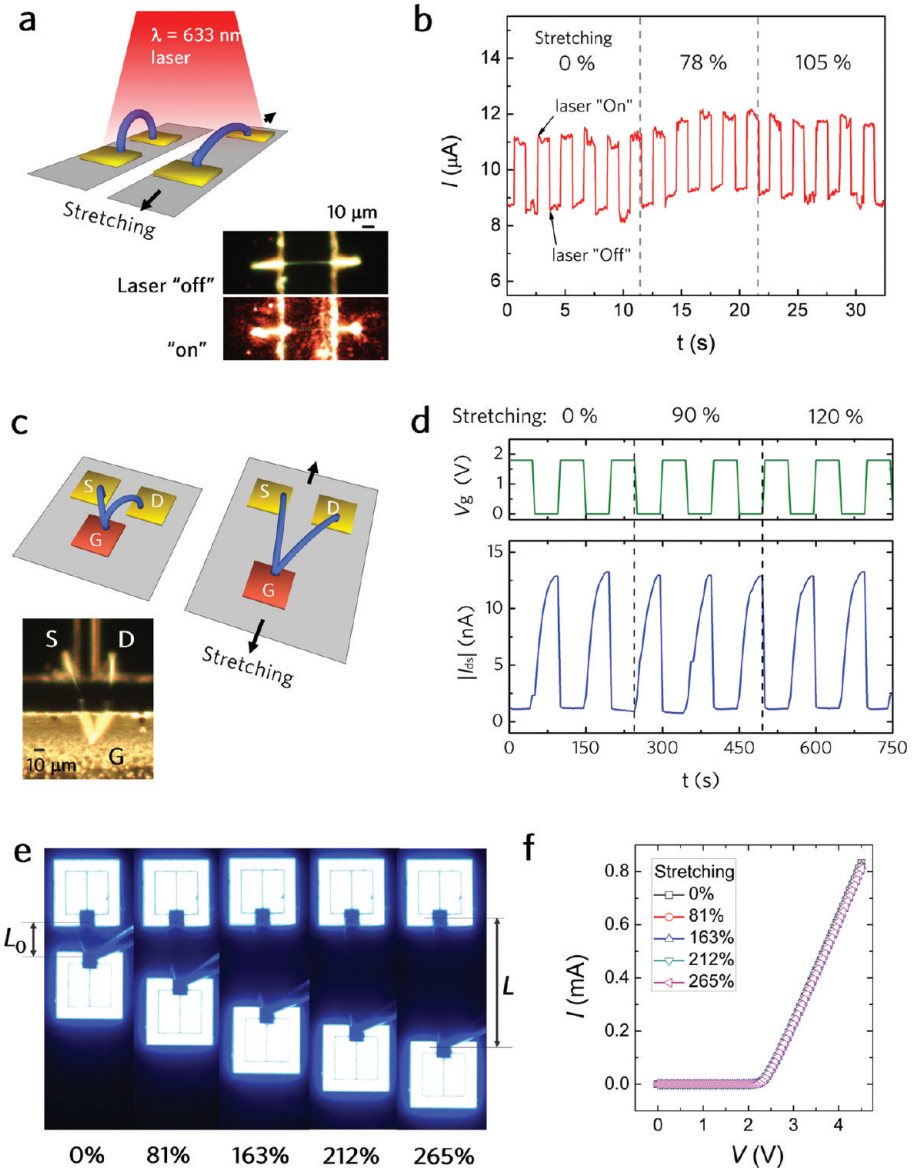

Figure 4. Highly stretchable organic electronic devices. (a, b) Photoswitches made of PEDOT/PSS nanoarches. (a) Schematic picture of an unstretched and stretched device. (b) Photocurrent vs time for 0, 78, and 105% stretching during a series of λ = 633 nm laser pulses in a dark box. (c, d) Electrochemical transistors (ECTs) with nanoarches. (c) Unstretched and stretched ECT: S = source, G = electrolyte gate, and D = drain. (d) Drain-source current I_{ds} vs time during the periodic 0−1.8 V switching of the gate voltage V_g for an ECT under different stretching conditions. (e, f) Operation of two LED chips connected to PEDOT/PSS arches: (e) Optical micrographs of the two LEDs under 4.5 V bias with zero and up to 265% stretching. (f) Current−voltage characteristics for different stretching conditions.

We fabricated ECTs with nanoarches connecting the source (S), the electrolyte-coated gate (G), and the drain (D) embedded in PDMS as schematically shown in Figure 4c (the detailed procedure is described in the Experimental Methods). The ECT operation is based on the conductivity switching of a transistor channel by a reversible redox reaction in the PEDOT/PSS in contact with the electrolyte[31] (the transport characteristics are shown in the Supporting Information, Figure S4a). The transistor is "on" for zero gate voltage but, when the gate voltage increases, the transistor channel is depleted and the transistor turns "off". The on/off ratio of drain-source current I_{ds} is >25 for low gate voltages of 0−1.8 V (Supporting Information, Figure S4b). The on/off switching (with ~25 ratio) was not affected by 90 and 120% stretching, as shown in Figure 4d. ECT like these could be used for stretchable ion-electron transducer interfaces between electronics and biological systems.[19]

Our stretchable 3D arches can be used not only for active components but also for electrical interconnections. Arches with 1.0 μm radius were used to obtain sufficient conductance. The performance was tested with light-emitting diode (LED) chips, as schematically illustrated in the Supporting Information, Figure S5. Optical images of two LEDs connected by PEDOT:PSS arches with $l_a/L_0 \sim 4.2$, with no stretch and during stretching up to 265% (Figure 4e) show that the arch-interconnections work well under extreme stretching conditions. This conclusion is corroborated by the current−voltage LED characteristics of Figure 4f, showing that the LED is "on" at an applied bias $\geq$2.3 V, consistent with the forbidden gap. Indeed, the current−voltage characteristics did not detectably change for 81, 163, 212, and 265% stretching.

dx.doi.org/10.1021/mz200249c | ACS Macro Lett. 2012, 1, 375−379

In summary, we demonstrated the use of direct 3D writing to fabricate not only stretchable PEDOT/PSS nanoelectronic components but also working devices. The performances of both the components and the devices did not change under extreme stretching conditions up to 270%. The fabrication technique is quite flexible and offers considerable latitude in controlling the component and device parameters: this is, we believe, a relevant step toward the full implementation of stretchable nanoelectronics.

EXPERIMENTAL METHODS

PEDOT/PSS writing: Two types of PEDOT/PSS solutions (Aldrich), 1.3 wt % (normal grade) and 2.2−2.6 wt % (high conductivity grade) in H_2O, were used to fabricate PEDOT/PSS nanostructures. To control the electrical conductivity, we added as a secondary dopant DMSO with 0.5−8.0 wt % concentration. Glass micropipets (r_0 = 750 nm) were fabricated with a pipet-puller (P-97 Sutter Instrument) and filled with the solution. The micropipet pulling was accurately controlled by *x*-*y*-*z* stepping motors (accuracy: 250 nm). For electrical stability, the nanoarches were annealed for 20 min at 120 °C after fabrication.

Electrochemical transistors (ECTs) demonstration: A PEDOT/PSS solution (1.3 wt %, Aldrich) with ethylene glycol (EG) 5 wt % was used for PEDOT/PSS writing. A gate substrate (Au) was coated with the PEDOT/PSS solution and then with an electrolyte using a spin coater. The electrolyte contained 33 wt % PSS, 12 wt % EG, 8 wt % sorbitol, water, and 0.1 molar $NaClO_4$. For source and drain electrodes, Au-coated Si wafers were used.

Characterizations: The tests of the products included FE-SEM (with a PHILIPS XL30SFEG), optical microscopy, stretchability measurements, electrical conductivity measurements, and photocurrent measurements. The stretchability was analyzed using a home-built test system. This was based on a stretchable substrate consisting of a conducting material (Au, Pt) separated by controlled gaps and embedded in PDMS. During stretching, current−voltage (*I*−*V*) characteristics of the LED chips and photoswitches and transport characteristics of the ECTs were recorded at room temperature with a Keithley 2612A instrument. The operation of the LED chips was visually monitored using an optical microscope. Photocurrents were generated using a 633 nm laser with 1.0 mW and a Keithley 2612A instrument (for the applied bias) in a dark box.

ASSOCIATED CONTENT

Supporting Information

Supporting figures (Figures S1−S5). This material is available free of charge via the Internet at http://pubs.acs.org.

AUTHOR INFORMATION

Corresponding Author

*E-mail: jhje@postech.ac.kr; giorgio.margaritondo@epfl.ch.

Notes

The authors declare no competing financial interest.

ACKNOWLEDGMENTS

This work was supported by the Creative Research Initiatives (Functional X-ray Imaging) of MEST/NRF and by the Swiss Fonds National pour la Recherche Scientifique and by the Center for Biomedical Imaging (CIBM). J.-H.A. acknowledges the support by the Basic Science Research Program (2011-0006268) of MEST/NRF.

REFERENCES

(1) Rogers, J. A.; Someya, T.; Huang, Y. *Science* **2010**, *327*, 1603−1607.
(2) Kim, D.-H.; Ahn, J. -H.; Choi, W. M.; Kim, H. -S.; Kim, T. -H.; Song, J.; Huang, Y. Y.; Liu, Z.; Lu, C.; Rogers, J. A. *Science* **2008**, *320*, 507−511.
(3) Ko, H. C.; Stoykovich, M. P.; Song, J.; Malyarchuk, V.; Choi, W. M.; Yu, C. -J.; Geddes, J. B. III; Xiao, J.; Wang, S.; Huang, Y.; Rogers, J. A. *Nature* **2008**, *454*, 748−753.
(4) Kim, D. -H.; Lu, N.; Ghaffari, R.; Kim, Y. -S.; Lee, S. P.; Xu, L.; Wu, J.; Kim, R. -H.; Song, J.; Liu, Z.; Viventi, J.; Graff, B.; Elolampi, B.; Mansour, M.; Slepian, M. J.; Hwang, S.; Moss, J. D.; Won, S. -M.; Huang, Y.; Litt, B.; Rogers, J. A. *Nat. Mater.* **2011**, *10*, 316−323.
(5) Sekitani, T.; Zschieschang, U.; Klauk, H.; Someya, T. *Nat. Mater.* **2010**, *9*, 1015−1022.
(6) Bae, S.; Kim, H.; Lee, Y.; Xu, X.; Park, J.-S.; Zheng, Y.; Balakrishnan, J.; Lei, T.; Kim, H. R.; Song, Y. I.; Kim, Y.-J.; Kim, K. S.; Özyilmaz, B.; Ahn, J.-H.; Hong, B. H.; Iijima, S. *Nat. Nanotechnol.* **2010**, *5*, 574−578.
(7) Lacour, S. P.; Jones, J.; Wagner, S.; Li, T.; Suo, Z. *Proc. IEEE* **2005**, *93*, 1459−1467.
(8) Ryu, S. Y.; Xiao, J.; Park, W. I.; Son, K. S.; Huang, Y. Y.; Paik, U.; Rogers, J. A. *Nano Lett.* **2009**, *9*, 3214−3219.
(9) Xu, F.; Lu, W.; Zhu, Y. *ACS Nano* **2011**, *5*, 672−678.
(10) Qi, Y.; Kim, J.; Nguyen, T. D.; Lisko, B.; Purohit, P. K.; McAlpine, M. C. *Nano Lett.* **2011**, *11*, 1331−1336.
(11) Sun, Y.; Choi, W. M.; Jiang, H.; Huang, Y. Y.; Rogers, J. A. *Nat. Nanotechnol.* **2006**, *1*, 201−207.
(12) Khang, D. -Y.; Xiao, J.; Kocabas, C.; MacLaren, S.; Banks, T.; Jiang, H.; Huang, Y. Y.; Rogers, J. A. *Nano Lett.* **2008**, *8*, 124−130.
(13) Ahn, J.-H.; Je, J. H. *J. Phys. D: Appl. Phys.* **2012**, in press.
(14) Ahn, B. Y.; Duoss, E. B.; Motala, M. J.; Guo, X.; Park, S.-I.; Xiong, Y.; Yoon, J.; Nuzzo, R. G.; Rogers, J. A.; Lewis, J. A. *Science* **2009**, *323*, 1590−1593.
(15) Gratson, G. M.; Xu, M.; Lewis, J. A. *Nature* **2004**, *428*, 386.
(16) Ahn, B. Y.; Shoji, D.; Hansen, C. J.; Hong, E.; Dunand, D. C.; Lewis, J. A. *Adv. Mater.* **2010**, *22*, 2251−2254.
(17) Na, S. -I.; Kim, S. -S.; Jo, J.; Kim, D. -Y. *Adv. Mater.* **2008**, *20*, 4061−4067.
(18) Cutler, C. A.; Bouguettaya, M.; Reynolds, J. R. *Adv. Mater.* **2002**, *14*, 684−688.
(19) Nilsson, D.; Robinson, N.; Berggren, M.; Forchheimer, R. *Adv. Mater.* **2005**, *17*, 353−358.
(20) Ramanathan, K.; Bangar, M. A.; Yun, M.; Chen, W.; Myung, N. V.; Mulchandani, A. *J. Am. Chem. Soc.* **2005**, *127*, 496−497.
(21) Simon, D. T.; Kurup, S.; Larsson, K. C.; Hori, R; Tybrandt, K.; Goiny, M.; Jager, E. W. H.; Berggren, M.; Canlon, B.; Richter-Dahlfors, A. *Nat. Mater.* **2009**, *8*, 742−746.
(22) Isaksson, J.; Kjäll, P.; Nilsson, D.; Robinson, N. D.; Berggren, M.; Richter-Dahlfors, A. *Nat. Mater.* **2007**, *6*, 673−679.
(23) Beh, W. S.; Kim, I. T.; Qin, D.; Xia, Y.; Whitesides, G. M. *Adv. Mater.* **1999**, *11*, 1038−1041.
(24) Zhang, F.; Nyberg, T.; Inganäs, O. *Nano Lett.* **2002**, *2*, 1373−1377.
(25) Lim, J. -H.; Mirkin, C. A. *Adv. Mater.* **2002**, *14*, 1474−1477.
(26) Li, M.; Guo, Y.; Wei, Y.; MacDiarmid, A. G.; Lelkes, P. I. *Biomaterials* **2006**, *27*, 2705−2715.
(27) Lang, U.; Dual, J. *Key Eng. Mater.* **2007**, *345*−*346*, 1189−1192.
(28) Kim, J. T.; Seol, S. K.; Pyo, J.; Lee, J. S.; Je, J. H.; Margaritondo, G. *Adv. Mater.* **2011**, *23*, 1968−1970.
(29) Nain, A. S.; Amon, C.; Sitti, M. *IEEE Trans. Nanotechnol.* **2006**, *5*, 499−510.
(30) Ghezzi, D.; Antognazza, M. R.; Maschio, M. D.; Lanzarini, E.; Benfenati, F.; Lanzani, G. *Nat. Commun.* **2011**, *2*, 166.
(31) Hamedi, M.; Forchheimer, R.; Inganäs, O. *Nat. Mater.* **2007**, *6*, 357−362.